Probing the Backbone Dynamics of Oxidized and Reduced Rat Microsomal Cytochrome b_5 via ^{15}N Rotating Frame NMR Relaxation Measurements: Biological Implications†

Lucia Banci, Ivano Bertini,* Christine Cavazza, Isabella C. Felli, and Dionysios Koulougliotis

Department of Chemistry, University of Florence, Via Gino Capponi 7, 50121 Florence, Italy

Received April 20, 1998; Revised Manuscript Received July 2, 1998

ABSTRACT: Rotating frame ^{15}N relaxation NMR experiments have been performed to study the local mobility of the oxidized and reduced forms of rat microsomal cytochrome b_5, in the microsecond to millisecond time range. Measurements of rotating frame relaxation rates ($R_{1\rho}$) were performed as a function of the effective magnetic field amplitude by using off-resonance radio frequency irradiation. Detailed analysis of the two data sets resulted in the identification of slow motions along the backbone nitrogens for both oxidation states of the protein. The local mobility of reduced and oxidized cytochrome b_5 turned out to be significantly different; 28 backbone nitrogens of the oxidized form were shown to participate in a conformational exchange process, while this number dropped to 12 in the reduced form. The correlation time, τ_{ex}, for the exchange processes could be determined for 21 and 9 backbone nitrogens for oxidized and reduced cytochrome b_5, respectively, with their values ranging between 70 and 280 μs. The direct experimental evidence provided in this study for the larger mobility of the oxidized form of the protein is consistent with the different backbone NH solvent exchangeability recently documented for the two oxidation states [Arnesano, F., et al. (1998) *Biochemistry 37*, 173−184]. Our experimental observations may have significant biological implications. The differential local mobility between the two oxidation states is proposed to be an important factor controlling the molecular recognition processes in which cytochrome b_5 is involved.

Solution structures obtained through NMR are quite relevant as they constitute the starting point for other studies; in particular, they can be further explored in terms of local mobility. In electron transfer proteins, the structure and mobility can be meaningfully compared between the two redox partners (*1*−*8*). This has become possible after the progress in the solution structure determination of paramagnetic molecules (*2*, *9*−*11*) since, in most cases, at least one redox partner in electron transfer proteins is paramagnetic (*12*). Mobility may be related to molecular recognition (*13*).

The solution structures of both oxidized and reduced rat microsomal cytochrome b_5 have recently become available (*7*, *8*). Cytochrome b_5 (cyt b_5 hereafter) is a largely widespread electron transfer protein found in a variety of mammalian and avian species, and it has been extensively studied (*12*, *14*, *15*). It contains a *b*-type heme which, together with two histidine side chains, provides the coordination sphere for the iron ion. The latter cycles between the +3 and +2 oxidation states. Since the heme is not covalently bound to the protein matrix, it is present in two orientations, usually indicated as the A (major) and B (minor) forms. The relative populations of the two forms vary according to the specific isoenzyme and are 6:4 in the rat microsomal isoenzyme. Cyt b_5 is mainly found as a membrane-bound protein (*16*). However, a hydrophilic domain can be identified. It can be either isolated through tryptic cleavage or expressed in *Escherichia coli*, and it still retains its activity (*16*−*19*). Due to its moderate dimensions as well as to the relatively easy procedure through which it can be obtained, it has become the subject of many studies with a variety of different methods. Therefore, it represents an ideal system for addressing fundamental problems related to how the electron transfer process occurs in living organisms (*20*−*22*) and, more generally, to how energy is transferred in living organisms. The careful comparison of the solution structures of cyt b_5 in both oxidation states (*7*, *8*) revealed small but significant differences indicating structural rearrangements that could be important in determining the stability of the protein in the two redox states and thus be related to the redox potential. Further inspection of NMR data revealed a differential behavior of the two redox states with respect to exchange of labile protons with the bulk solvent (*7*). Since the structure of the protein in the two oxidation states is not so different to justify a different solvent accessibility, this fact could be interpreted as being due to differential mobility in the two oxidation states (*7*), which would produce different instantaneous accessibility. Local mobility has often been thought, from indirect evidence, to be important in controlling the electron

† This work was supported by the European Community (Program BIOMED, CT BMH4-CT96-1492), the Italian CNR (Biotecnologie e biologia molecolare, CTB CNR 95.02860.CT14), and MURST-ex 40%. D.K. thanks the TMR Programme of the European Union for a postdoctoral fellowship (Contract ERBFMBICT960994).

* Corresponding author: Department of Chemistry, University of Florence, Via Gino Capponi 7, 50121 Florence, Italy. Fax: +39 55 2757555. Telephone: +39 55 2757549. E-mail: bertini@lrm.fi.cnr.it.

S0006-2960(98)00885-X CCC: $15.00
Published on Web 08/08/1998

transfer process (*22*−*27*). Local mobility can indeed influence the molecular recognition process (*13*, *28*−*31*) as well as the reorganization energy λ (*20*−*22*), both features being necessary to achieve electron transfer in biological systems. Moreover, differential mobility of some regions of the protein can provide insight about the recognition process between the two redox partners and in the electron transfer process (*7*). However, direct experimental evidence of local mobility for electron transfer proteins in both oxidation states is still quite rare (*32*−*34*). Therefore, a further characterization of the local mobility of cyt b_5 in both oxidation states could provide useful information.

Analysis of heteronuclear NMR relaxation has revealed a unique method for obtaining information on local mobility (*35*−*37*). In particular, rotating frame relaxation experiments have recently attracted the attention of several researchers (*38*−*40*) due to their potential to reveal motions in an intermediate time range, that is from microseconds to milliseconds (*36*, *41*−*45*). This method has recently been applied on the HiPIP I from *Ectothiorhodospira halophila*, and it allowed the identification of a loop exhibiting an exchange process (*46*).

We report here a characterization of the local mobility of rat microsomal cyt b_5 in both oxidation states, in the microsecond to millisecond time range, by exploiting ^{15}N off-resonance rotating frame relaxation.

EXPERIMENTAL PROCEDURES

Sample Preparation. ^{15}N-labeled cyt b_5 was isolated and purified as previously described (*16*) from cultures of *E. coli* strain TOPP 1 harboring the recombinant pUC13 plasmid containing the gene encoding the 98-amino acid polypeptide corresponding to the soluble part of rat microsomal cyt b_5 (kindly provided by S. G. Sligar). The cultures were grown in minimal M9 medium containing $(^{15}NH_4)_2SO_4$ (3 g/L) as the sole nitrogen source. After cell lysis with sonication, the purification was carried out in two steps, including a CL-6B anion exchange column followed by a P100 (Bio-Rad) chromatography column. Approximately 15 mg of pure protein (obtained from a 5 L culture) was exchanged through ultrafiltration (YM10 membranes, Amicon) with 10 mM phosphate buffer at pH 7.0. The sample volume was reduced to ca. 500 μL with a final concentration of ca. 3 mM. Under these conditions, the majority of the protein (>95%) is in the oxidized form. To keep the protein in the oxidized state over the course of several days (needed for the performance of the NMR experiments), the NMR tube was periodically (every 40−45 h) flashed with oxygen for 10−15 min. The protein was reduced by the anaerobic addition of 20 μL of 1 M sodium dithionite solution buffered at pH 6.9 (10 mM phosphate).

NMR Experiments. All NMR experiments were carried out at 298 K, on a Bruker Avance 600 NMR spectrometer operating at a proton Larmor frequency of 600.13 MHz.

The ^{15}N off-resonance rotating frame relaxation rates ($R_{1\rho}^{OFF}$) were measured as a function of the effective magnetic field amplitude (ω_{eff}) by using the pulse sequence described recently (*39*). The ^{15}N RF irradiation was applied with an amplitude ω_1 and with an offset $\Delta\omega$ with respect to the center of the amide nitrogen resonances to lock the magnetization along an axis making an angle $\theta = \arctan(\Delta\omega/\omega_1) = 35°$ with a resulting effective magnetic field amplitude ω_{eff}. The amplitude of the ^{15}N RF irradiation during the pulse sequence was increased and decreased gradually in a trapezoidal fashion to achieve adiabatic rotation of the magnetization to the effective magnetic field axis (*39*). During the application of the continuous wave spin-lock field at the ^{15}N frequency, decoupling of the protons is achieved with the Waltz-16 pulse decoupling sequence (*47*) to avoid creation of antiphase ^{15}N magnetization via cross-correlation processes (of the type N_xI_z, where N and I are the nuclear spin operators of the ^{15}N and the directly bound ^{1}H nuclei, respectively). The decoupling power was set to 2670 Hz in all experiments. The INEPT transfer delay was set to 2.5 ms (*48*). The applied effective magnetic field amplitude values ω_{eff} for the measurement of $R_{1\rho}^{OFF}$ were as follows: 1870, 2090, 2300, 2590, 2890, 3210, and 3550 Hz. For each spin-lock power, a series of two-dimensional (2D) experiments was performed in which the relaxation delay T was set to the following values: 10, 20, 36, 50, 60, 86, 100, 150, 200, 300, and 10 ms. A further 2D spectrum without the period of spin-lock field was also acquired to measure the initial magnetization. All experiments were recorded with a spectral width of 2130 Hz in the F_1 (^{15}N frequency) dimension and of 8390 Hz in the F_2 (^{1}H frequency) dimension. A total of 160 experiments in t_1, each of 2048 real data points, were recorded. Every free induction decay was comprised of 16 scans. Quadrature detection in F_1 was obtained by using the TPPI method of Marion and Wüthrich (*49*).

The longitudinal relaxation rate, R_1, was measured via an inversion recovery experiment of the ^{15}N nuclear spin introduced to a 2D heteronuclear correlation spectrum as described by Peng and Wagner (*50*). The following relaxation delays were used: 5, 10, 20, 40, 80, 120, 240, 320, 500, 1000, and 1500 ms. The acquisition parameters were equivalent to those used for the $R_{1\rho}^{OFF}$ measurement except that a total of 192 experiments were recorded for each 2D spectrum, each being comprised of eight scans.

Sequence-specific assignments of cyt b_5 in both oxidation states were available in the literature (*7*, *8*, *51*, *52*).

Data Processing. All 2D NMR data were processed on a Silicon Graphics workstation using the Xwinnmr Bruker software. Only the downfield part of the spectra (in the ^{1}H dimension), containing the H_N−N connectivities (5−12 ppm), was kept for the data analysis. All spectra were transformed with 4K × 1K points in the F_2 and F_1 dimensions, respectively. All spectra acquired with a common spin-lock power were processed by using the same processing parameters (phasing parameters, baseline correction, etc.). Subsequent integration of cross-peaks for all spectra was performed by using the standard routine available from Bruker.

Determination of Relaxation Rates. Relaxation rates R_1 and $R_{1\rho}^{OFF}$ were determined by fitting the cross-peak intensities (I) measured as a function of the relaxation delay T to a single-exponential decay by using the Levenberg−Marquardt algorithm (*53*, *54*) according to the following equation:

$$I(T) = A + B\exp(-RT) \quad (1)$$

A, B, and R are adjustable fitting parameters. A program

which uses a Monte Carlo approach (*39*, *55*, *56*) to estimate via the Levenberg−Marquardt algorithm the rates and their errors was used for this purpose. For $R_{1\rho}^{OFF}$, the phase cycle was chosen so that the magnetization relaxes to zero for long relaxation delays. Thus, in this case, A was set equal to zero in the fitting procedure. The error bars correspond to the experimental error averaged over all powers. The error value for $R_{1\rho}^{OFF,cor}$ (see later) includes the errors in the measurement of both $R_{1\rho}^{OFF}$ and R_1.

Analysis of Relaxation Rates. The magnetization of a ^{15}N spin i, when an RF irradiation of frequency ω and amplitude ω_1 is applied in the vicinity of its resonance frequency ω_i, is aligned along the effective magnetic field, which is characterized by an amplitude $\omega_{eff,i}$ of $(\Delta\omega_i^2 + \omega_1^2)^{1/2}$ and a direction making an angle θ_i of $\arctan(\omega_1/\Delta\omega_i)$ with the static magnetic field axis. The relaxation rate $R_{1\rho}^{OFF}$ of the ith spin along the effective magnetic field is given by the following expression (*40*, *44*, *57*, *58*)

$$R_{1\rho}^{OFF} = R_1 \cos^2\theta_i + R_{1\rho}^{ON,\infty} \sin^2\theta_i + K \sin^2\theta_i \frac{\tau_{ex}}{1 + \tau_{ex}^2 \omega_{eff,i}^2} \quad (2)$$

in the presence of chemical and/or conformational exchange between two conformations and a fast regime with respect to the chemical shift separation, i.e., $\delta\Omega\tau_{ex} \ll 1$, where $\delta\Omega$ is the chemical shift difference between the resonating nucleus in the two sites. The variables have the following meanings. R_1 is the longitudinal relaxation rate of the ith spin. $R_{1\rho}^{ON,\infty}$ is the on-resonance rotating frame relaxation rate of the ith spin for an infinitely large effective field amplitude (where all exchange contributions are dispersed to zero). τ_{ex} is the correlation time for the exchange process involving the ith spin. K is a constant equal to $p_a p_b \delta\Omega^2$, where p_a and p_b are the relative populations of the two states a and b, respectively, between which the exchange process occurs. Even if the rates and τ_{ex} are of course relative to a specific spin i, this will not be indicated explicitly so the nomenclature can be kept as simple as possible.

If the angle θ_i were kept constant, a dependence of $R_{1\rho}^{OFF}$ on ω_{eff} would be indicative of the presence of an exchange process involving the ^{15}N nucleus under investigation. However, for an applied RF irradiation with an amplitude ω_1, the angle θ_i will be strictly constant only for one spin i with frequency ω_i. Therefore, for all the other spins, when $R_{1\rho}^{OFF}$, R_1, and i are known, the following correction should be applied:

$$\frac{R_{1\rho}^{OFF} - R_1 \cos^2\theta_i}{\sin^2\theta_i} = R_{1\rho}^{ON,\infty} + K\frac{\tau_{ex}}{1 + \tau_{ex}^2 \omega_{eff,i}^2} = R_{1\rho}^{OFF,cor} \quad (3)$$

Thus, information on fast exchange processes can be obtained from the dependence of $R_{1\rho}^{OFF,cor}$ on the effective magnetic field amplitude. If the experimental $R_{1\rho}^{OFF,cor}$ values are fit to a Lorentzian function (eq 3), the correlation time τ_{ex} for the exchange process can be estimated. If, on the other hand, no exchange process is present, $R_{1\rho}^{OFF,cor}$ is independent of ω_{eff}. The lower limit value for $R_{1\rho}^{OFF,cor}$ is $R_{1\rho}^{ON,\infty}$ when $\omega_{eff,i}\tau_{ex} \gg 1$, i.e., $\tau_{ex} \gg 10^{-4}$ s (for the ω_{eff} used in this work), and the upper limit is $R_{1\rho}^{ON,\infty} + K\tau_{ex}$ when $\omega_{eff,i}\tau_{ex} \ll 1$, i.e., $\tau_{ex} \ll 10^{-4}$ s (in the limit of $\omega_{eff} \rightarrow 0$, $R_{1\rho}^{ON,\infty} \rightarrow R_2$). In addition, $\delta\Omega\tau_{ex} \ll 1$ must always hold. These limits are of help in determining τ_{ex} from the experimental data even if the latter values span a limited part of the Lorenzian curve. In our particular case, since ω_{eff} ranges between 1870 and 3550 Hz, we have access to τ_{ex} values in the range of approximately 10−300 μs. A dependence of $R_{1\rho}^{OFF,cor}$ on ω_{eff} is an indication of the presence of an exchange process; however, the estimate of τ_{ex} is not very accurate for τ_{ex} values larger than approximately 150 μs, and the data on τ_{ex} are discussed qualitatively (see later).

RESULTS

The off-resonance rotating frame relaxation rate, $R_{1\rho}^{OFF}$, was determined for each amide backbone ^{15}N spin at seven different effective magnetic field amplitudes, ω_{eff}. Except if differently indicated, the data are reported and analyzed for the A form of the protein. The experiments were performed by changing simultaneously the values of ω_1 and $\Delta\omega$ ($\Delta\omega$ is the offset between the frequency of the applied RF field and the center frequency of the amide region) to keep the angle $\theta = \arctan(\Delta\omega/\omega_1) = 35°$ for a nitrogen spin resonating at a frequency corresponding to the center of the amide region. For ^{15}N spins resonating at a different frequency, the angle θ_i will undergo a small but systematic variation corresponding to the changes in the values of ω_1 and $\Delta\omega_i$. This was accounted for, as described above, to obtain $R_{1\rho}^{OFF,cor}$ values according to eq 3. These values are hereafter analyzed.

For rat microsomal cyt b_5, the largest increases in θ_i between the lowest and highest values of ω_1 used were 4° and 4.8° (for the amide spin of residue 52) for the reduced and oxidized forms, respectively. The largest decreases in θ_i were 14.6° (reduced cyt b_5) and 14° (oxidized cyt b_5), for the backbone amide of residue 94. It should be noted, however, that the angular dispersion in the rotating frame (off-resonance) is always smaller than the corresponding dispersion when on-resonance irradiation is applied. The results on $R_{1\rho}^{OFF,cor}$ are discussed below separately for each oxidation state of cyt b_5.

Oxidized Cyt b_5. The longitudinal relaxation rates R_1 for 68 backbone amide nitrogen spins, which could be precisely integrated as they are not overlapping with other signals, are shown in Figure 1A. These rates display a uniform behavior along the protein sequence, and their average value is 1.9 ± 0.1 Hz, consistent with previously reported data on the bovine isoenzyme (*59*). These values were subsequently used in eq 3 to obtain $R_{1\rho}^{OFF,cor}$ values.

The dependence of $R_{1\rho}^{OFF,cor}$ on ω_{eff} was examined for each of the 68 backbone amides, and for 47 of these, the $R_{1\rho}^{OFF,cor}$ values were found independent of the effective magnetic field amplitude. The average values of $R_{1\rho}^{OFF,cor}$ (estimated using all the values obtained at the seven effective magnetic field amplitudes employed in the experiments) for the 47 backbone amides, which were found independent of ω_{eff}, are shown in Figure 2A (unmarked residues). These relaxation rates show overall a quite uniform behavior with an average value for $R_{1\rho}^{OFF,cor} = R_{1\rho}^{ON,\infty} = 6.8 \pm 0.9$ Hz, except of the ones corresponding to the backbone nitrogens of residues 27, 31,

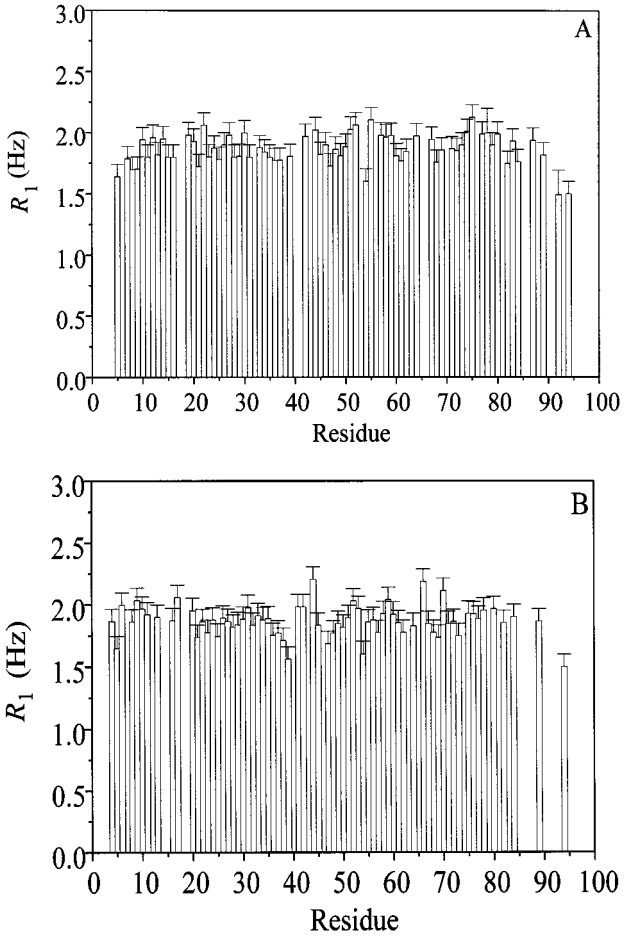

FIGURE 1: Longitudinal relaxation rates of ^{15}N backbone amides per residue for the oxidized (A) and reduced (B) forms of cyt b_5.

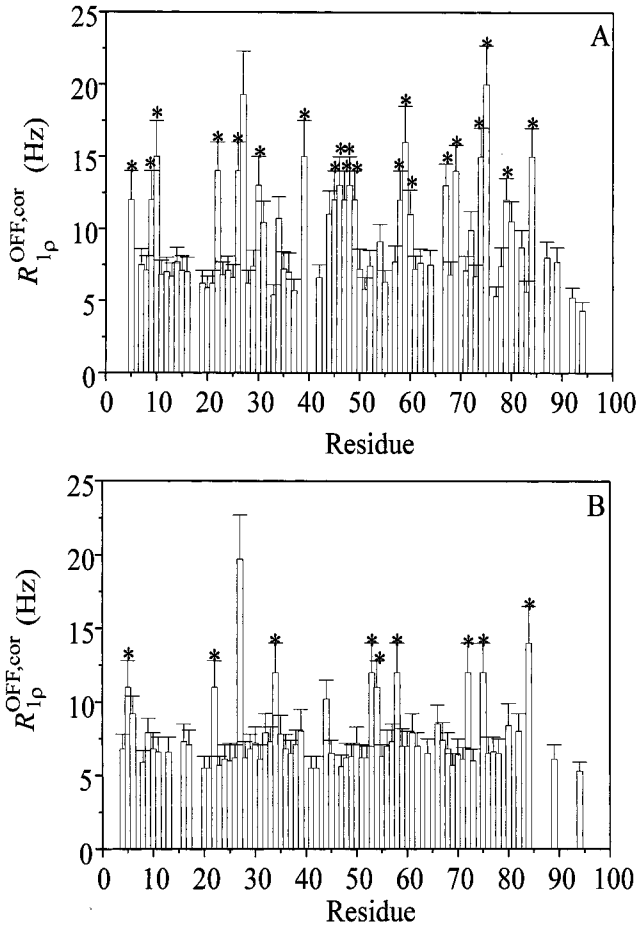

FIGURE 2: Off-resonance rotating frame ^{15}N relaxation rates, $R_{1\rho}^{OFF,cor}$, are reported per residue for the oxidized (A) and reduced (B) forms of cyt b_5. The rates marked with an asterisk showed a dependence of $R_{1\rho}^{OFF,cor}$ on ω_{eff}. For these residues, the rate corresponding to the lowest effective magnetic filed amplitude is reported.

34, 44, 54, 72, and 80. The latter seven residues have $R_{1\rho}^{OFF,cor}$ rates which are 40−150% larger than those of the remaining 40. An increase in $R_{1\rho}^{ON,\infty}$ due to higher "rigidity" of the NH bond vector in the sub-nanosecond time scale should be smaller than 40% (on the order of 25%), and thus, the data obtained for the above seven residues can be interpreted in terms of exchange processes.

These findings can be interpreted as follows. For the 40 residues with a uniform relaxation rate $R_{1\rho}^{OFF,cor}$ (6.8 ± 0.9 Hz), one can conclude either that there is no exchange process ($\tau_{ex} = 0$) or that it is not large enough to sizably contribute to $R_{1\rho}$. On the other hand, the behavior observed for the other seven residues can be an indication of the presence of a conformational exchange process. However, its time scale is faster that the one accessible with the available powers of the spin-lock field (ω_{eff}), and thus, $R_{1\rho}^{OFF,cor}$ appears to be constant as a function of ω_{eff} but with a higher value than in the absence of an exchange process. Since the highest effective magnetic field corresponds to a frequency of 3550 Hz, the exchange process operating for residues 27, 31, 34, 44, 54, 72, and 80 should have a correlation time τ_{ex} of $<$40 μs and a value of $\delta\Omega$ that is large enough so that $K\tau_{ex}$ is not negligible with respect to $R_{1\rho}^{ON,\infty}$ (6.8 ± 0.9 Hz).

By knowing the average value of R_1 and the average value of $R_{1\rho}^{OFF,cor}$ for residues that are not involved in exchange processes, if we approximate that $R_{1\rho}^{OFF,cor}$ equals R_2, we can determine the overall rotational correlation time, τ_c, of the protein from the ratio R_2/R_1 (*60*). Provided $J(\omega_H)$ is negligible with respect to $J(\omega_N)$ and $J(0)$, which is quite reasonable at the high magnetic field at which measurements are performed:

$$\frac{R_2}{R_1} \approx {}^2/_3 \frac{J(0)}{J(\omega_N)} + {}^1/_2 \quad (4)$$

where $\nu_N \approx 60.8$ MHz and it holds that

$$\frac{J(0)}{J(\omega_N)} = 1 + \omega_N{}^2\tau_c{}^2 \quad (5)$$

Since the average values of $R_{1\rho}^{OFF,cor}$ and R_1 for all 40 ^{15}N backbone amides that display uniform relaxation rates in the rotating frame are 6.8 ± 0.9 and 1.9 ± 0.1 Hz, respectively, we can determine a value for τ_c of 5.0 ± 0.7 ns. This value is consistent with the one estimated in a recent study on the backbone dynamics of oxidized bovine microsomal cyt b_5 (*59*), and it also lies in the range of that estimated through the Stokes−Einstein equation (*61*) which turns out to be 3.6 ± 1.3 ns.

Conformational Exchange Processes in Oxidized Cyt b_5. The $R_{1\rho}^{OFF,cor}$ values for the remaining 21 nitrogen backbone amides showed a dependence on the effective magnetic field

Table 1: Exchange Correlation Times (τ_{ex}) Estimated for Amide Backbone Nitrogens of Oxidized and Reduced Cyt b_5[a]

residue	secondary element	oxidized cyt b_5 τ_{ex} (μs)	reduced cyt b_5 τ_{ex} (μs)
Lys 5	β1	180 ± 30	190 ± 30
Tyr 6	β1	*b*	<40
Leu 9	α1	70 ± 15	−
Glu 10	α1	280 ± 50	−
Trp 22	β4	170 ± 30	180 ± 30
His 26	turn	180 ± 30	−
His 27	turn	<40	<40
Tyr 30	β3	110 ± 20	−
Asp 31	β3	<40	−
Lys 34	α2	<40	200 ± 30
His 39	α2	190 ± 30	−
Glu 44	α3	<40	<40
Val 45	α3	180 ± 30	−
Leu 46	α3	190 ± 30	*b*
Arg 47	α3	200 ± 30	−
Glu 48	α3	280 ± 50	−
Gln 49	α3	200 ± 30	−
Asp 53	turn	*b*	190 ± 30
Ala 54	α4	<40	140 ± 25
Phe 58	α4	150 ± 25	220 ± 35
Glu 59	α4	110 ± 20	−
Asp 60	α4	200 ± 30	−
Ala 67	α5	200 ± 30	−
Glu 69	α5	180 ± 25	−
Lys 72	α5	<40	170 ± 25
Tyr 74	α5	180 ± 25	*b*
Ile 75	β2	70 ± 15	165 ± 25
Leu 79	turn	220 ± 40	*b*
His 80	turn	<40	−
Arg 84	α6	190 ± 30	220 ± 30

[a] The secondary structural elements to which each amide belongs are also reported. [b] Amide backbone nitrogens for which a relaxation rate could not be evaluated due to overlap in the spectra.

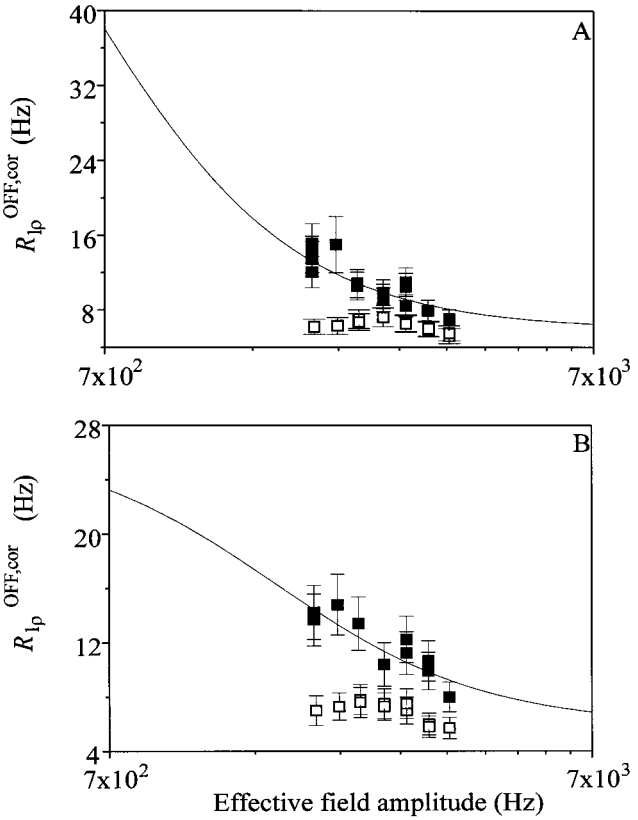

FIGURE 3: Off-resonance rotating frame relaxation rates for two residues, Glu 48 (A) and Glu 59 (B), as a function of the effective magnetic field amplitude ω_{eff}, for the oxidized (■) and reduced (□) forms of rat microsomal cyt b_5. The solid curves represent the fit with the function of eq 3 ($R_{1\rho}^{ON,\infty}$ = 5.9 and 5.8 Hz for the oxidized and reduced forms, respectively).

amplitude ω_{eff}. More specifically, they displayed a monotonic increase with decreasing ω_{eff}, reaching values, for two residues, up to 15 Hz at the lowest ω_{eff} employed (1870 Hz). In Figure 2A, the rates $R_{1\rho}^{OFF,cor}$ measured at 1870 Hz for these 21 backbone amides are reported. These correspond to residues 5, 9, 10, 22, 26, 30, 39, 45−49, 58−60, 67, 69, 74, 75, 79, and 84. They have been marked with an asterisk to differentiate them from the remaining 47 amides whose $R_{1\rho}^{OFF,cor}$ relaxation rates were independent of ω_{eff}.

The relaxation behavior observed for these residues provides direct experimental evidence for the presence of exchange processes. Their correlation times τ_{ex} can be obtained by performing a fit of the data to eq 3. This was achieved successfully for all 21 residues. The fits were performed by using the nonlinear fitting routine provided by the Levenberg−Marquardt algorithm. The values estimated for τ_{ex} varied between 70 (for Leu 9 and Ile 75) and 280 μs (for Glu 48) and are reported in Table 1. It should be noted that in these fits, K and τ_{ex} were adjustable parameters while a fixed value was used for $R_{1\rho}^{ON,\infty}$. This value was equal to 5.9 Hz and corresponds to the lower limit of the average $R_{1\rho}^{OFF,cor}$ (6.8 ± 0.9 Hz) obtained, as described above, for the 40 residues not involved in exchange processes. The fits were also performed by using 7.7 Hz (the upper limit of $R_{1\rho}^{ON,\infty}$) as the fixed value of $R_{1\rho}^{ON,\infty}$. The correlation times extracted were systematically 20−25% larger, and a uniform systematic increase (∼5%) was also obtained for their errors. In some cases, an initial estimate for τ_{ex} was used so we were able to obtain a reasonable starting value for the parameter K, and then these two parameters were allowed to change alternatively in an iterative way until convergence of the fit was reached. The obtained parameters were compared with the limit at low $\omega_{eff,i}$ values, i.e., $R_{1\rho}^{OFF,cor} = R_2$ where an estimate of R_2 was obtained from the line widths. In all cases, the K values were consistent with the expected low $\omega_{eff,i}$ limits. An analogous fitting procedure was also applied to the reduced form and produced similar results (see later). Two representative fits corresponding to the backbone nitrogens of residues Glu 48 and Glu 59 are shown in Figure 3. In addition, the data for Ile 75 are shown in Figure 4A. The correlation times for the exchange process in which they participate are 280 ± 50, 110 ± 20, and 70 ± 15 μs, respectively. These residues were chosen as being representative of the entire time range that can be probed with the current experimental setting.

In summary, 28 backbone nitrogens in the oxidized state of rat microsomal cyt b_5 were identified to participate in conformational exchange processes in the microsecond to millisecond time scale. A large amount of residues involved in exchange processes was also suggested in a previous study of the oxidized bovine isoenzyme (*59*), but no definitive conclusions were reached. The correlation time for the process could be determined for 21 residues, while for the remaining seven, only an upper limit (40 μs) can be estimated. The results for all 28 residues are reported in Table 1 together with the secondary structural elements of the protein to which they belong.

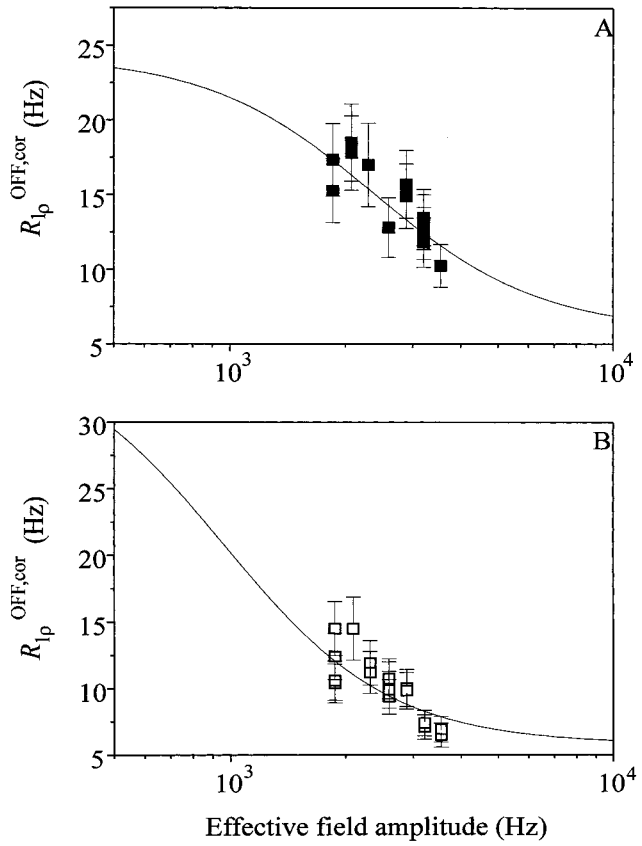

FIGURE 4: Off-resonance rotating frame relaxation rates for Ile 75 are shown as a function of the effective magnetic field amplitude ω_{eff}, for the oxidized (A) and reduced (B) forms of rat microsomal cyt b_5. The solid curves represent the fit with the function of eq 3 ($R_{1\rho}^{ON,\infty} = 5.9$ and 5.8 Hz for the oxidized and reduced forms, respectively).

Reduced Cyt b_5. The longitudinal relaxation rates R_1 for 68 nitrogen backbone amides that could be precisely integrated are shown in Figure 1B. They turn out to be very similar to those of the oxidized form (Figure 1B) and display overall a uniform behavior along the protein sequence with an average value of 1.9 ± 0.1 Hz, i.e., the same as for the oxidized form.

The relaxation rates $R_{1\rho}^{OFF,cor}$ were analyzed with the same approach described for the oxidized form. For 59 (out of 68) residues, the values of $R_{1\rho}^{OFF,cor}$ were independent of the spin-lock power used. Their average values of $R_{1\rho}^{OFF,cor}$ (estimated using all the values obtained at the seven effective magnetic field amplitudes employed in the experiments) are shown in Figure 2B (unmarked). These rates show overall a uniform behavior with an average value for $R_{1\rho}^{OFF,cor}$ of 6.7 ± 0.9 Hz, except for those of the backbone nitogens of residues 6, 27, and 44. For these three residues, the $R_{1\rho}^{OFF,cor}$ rates are 40−150% larger that the remaining 56.

We can thus conclude that the 56 residues with a uniform relaxation rate $R_{1\rho}^{OFF,cor}$ in the range 6.7 ± 0.9 Hz do not participate in any exchange process ($\tau_{ex} = 0$) or that if they do, it is not large enough to sizably contribute to $R_{1\rho}$. On the other hand, the relaxation behavior of residues 6, 27, and 44 indicates the presence of a conformational exchange process with a correlation time τ_{ex} of <40 μs, and a value of $\delta\Omega$ that is large enough so that $K\tau_{ex}$ is not negligible with respect to $R_{1\rho}^{ON,\infty}$ (6.7 ± 0.9 Hz).

By using eqs 4 and 5, the overall rotational correlation time, τ_c, for the reduced form of the protein is 4.9 ± 0.7 ns, which is the same as that determined for the oxidized form.

Conformational Exchange Processes in Reduced Cyt b_5. The relaxation rates $R_{1\rho}^{OFF,cor}$ for the nine remaining residues, corresponding to residues 5, 22, 34, 53, 54, 58, 72, 75, and 84, showed a dependence on the effective magnetic field amplitude ω_{eff}. The rates $R_{1\rho}^{OFF,cor}$ for these nine residues measured at the lowest spin-lock power employed (1870 Hz) are displayed in Figure 2B and marked with an asterisk.

Again, the dependence of $R_{1\rho}^{OFF,cor}$ on ω_{eff} indicates the presence of conformational exchange processes. The experimental values of $R_{1\rho}^{OFF,cor}$ were fit to eq 3, as already described for the oxidized form, thus evaluating the exchange correlation times, τ_{ex}, for all nine residues. τ_{ex} values varied between 140 (Ala 54) and 220 μs (Phe 58) and are reported in Table 1. $R_{1\rho}^{ON,\infty}$ was set equal to 5.8 Hz, which corresponds to the lower limit of the average $R_{1\rho}^{ON,\infty}$ (6.7 ± 0.9 Hz). A representative fit is shown in Figure 4B and corresponds to the backbone nitrogen of residue Ile 75 (τ_{ex} = 165 ± 25 μs).

In the reduced form of cyt b_5, only 12 backbone nitrogens were involved in conformational exchange processes on the microsecond to millisecond time scale. The correlation time for the process could be accurately determined for nine residues, while for the three remaining residues, only an upper limit (40 μs) could be estimated. The results for all 12 residues are reported in Table 1 together with those for the oxidized form.

DISCUSSION

A Comment on the Possible Effects of Unpaired Electrons. The oxidized form of cyt b_5 is paramagnetic, and thus, the effect of the low-spin heme Fe(III) on proton relaxation is expected to be non-negligible (*62*−*64*). However, the effect on nitrogen relaxation is dramatically reduced (approximately by a factor of 100) due to the lower gyromagnetic ratio of the ^{15}N with respect to the ^{1}H nucleus (lower by a factor of 10). Recently (*46*), off-resonance rotating frame ^{15}N relaxation measurements were employed to probe the backbone dynamics of the reduced recombinant HiPIP I from *E. halophila*, which is a highly paramagnetic protein at room temperature (*65*). In that case, a lower limit for the paramagnetic contribution on the rotating frame relaxation rates was estimated. It was shown that the effect is non-negligible only for ^{15}N nuclei closer than 7 Å to at least one of the iron atoms of the 4Fe-4S cluster. The low-spin heme Fe(III) ion is expected to enhance the nuclear relaxation rates less than the coupled polymetallic cluster of reduced HiPIPs as its electron relaxation rates are shorter. From the longitudinal relaxation rates of the heme methyl signals (*66*) [which are at a fixed distance of 6.1 Å from the Fe(III) atom], an electronic relaxation time τ_s of about 7 × 10^{-12} s is estimated for the low-spin heme Fe(III). All ^{15}N nuclei that displayed "slow" dynamic modes are more than 7 Å from the heme iron. The closest backbone ^{15}N nuclei, as determined from the average energy-minimized solution structure of the oxidized protein (*7*), are those of His 39 (7.6 Å), Leu 46 (7.4 Å), Phe 58 (7.5 Å), and Ala 67 (7.8 Å). For such distances, the paramagnetic contibution on ^{15}N longitudinal relaxations is estimated to be in the range of 0.02−

0.05 Hz, which is very small and within the experimental uncertainty. Indeed, the longitudinal relaxation rates measured for the latter four residues in the oxidized form of cyt b_5 were 1.8 ± 0.1, 1.9 ± 0.1, 2.0 ± 0.1, and 1.9 ± 0.1 Hz, respectively. Similar rates, within experimental error, were measured for the same residues also in the reduced form of cyt b_5 (1.6 ± 0.1, 1.9 ± 0.1, and 1.9 ± 0.1 Hz for His 39, Phe 58, and Ala 67, respectively, while Leu 46 was not well resolved and thus its R_1 rate could not be accurately determined). Therefore, in the case of oxidized cyt b_5, the effect of paramagnetic relaxation on ^{15}N R_1 relaxation is negligible. This makes the analysis of the experimental data more straightforward, and exchange processes on the microsecond to millisecond time range can be safely probed also in the presence of a paramagnetic center.

Another additional effect on NMR parameters, due to the presence of a paramagentic center, is the pseudocontact contribution to the chemical shift (*62*). The method for revealing chemical or conformational exchange processes from the $R_{1\rho}$ measurements as a function of the effective magnetic field amplitude relies on the existence of a difference in chemical shift, $\delta\Omega$, between the two states involved in the exchange process. Therefore, possible additional contributions to the chemical shift, due to the paramagnetic center, should be critically evaluated. Particularly significant is the pseudocontact contribution, which depends on the position of the nucleus with respect to the origin and the axes of the magnetic susceptibility tensor. For example, a specific ^{15}N nucleus participating in an exchange process would experience a fairly small change in the "diamagnetic" chemical shift, whereas the variation due to the pseudocontact shift could be much larger. Consequently, the total $\delta\Omega$ would be non-negligible, and the exchange process could be experimentally probed. In other words, the pseudocontact contribution to the chemical shift could "illuminate" small amplitude motions that would be invisible in the absence of such contribution. This could be one of the reasons why many more exchange processes were detected in the oxidized form (the paramagnetic one) of cyt b_5. If that were the case, then our experimental observations could not be interpreted solely in terms of an oxidation state-dependent mobility of the two forms of the protein. Therefore, it is necessary to try to give an estimate of the pseudocontact contribution to the effective $\delta\Omega$. The pseudocontact contribution to the chemical shift is independent of the gyromagnetic ratio of the nucleus. In addition, the ^{15}N chemical shift range for amide nitrogens in the reduced protein is on the order of 25 ppm, while the pseudocontact shift range experimentally observed in this case is on the order of 2 ppm. Thus, the pseudocontact contribution to the observed ^{15}N chemical shift values is much smaller than the diamagnetic one. However, what is relevant is the change in the pseudocontact shift induced by the presence of a conformational exchange process. A rough estimation of the variation of the pseudocontact shift with the conformation can be given by the range of pseudocontact shifts (*67*) experienced by each amide proton within the family of 40 structures of the oxidized form of the protein (*7*). The largest calculated variations (approximately 0.6 ppm) were observed for the NHs of residues 46, 58, 59, and 67. On the other hand, the change in the shift for the possible conformations can be estimated from the fits of the experimental data by using eq 3. By assuming an equal population of the two exchanging conformations ($p_a p_b = 0.25$), one can estimate, from the parameter K, $\delta\Omega$ which results in the range of 2.1−2.8 ppm for both oxidation states. For the NHs of residues 46, 58, 59, and 67, which are the ones that are most affected by the pseudocontact contribution, this value turned out to be close to 2.5 ppm. Thus, one could estimate a contribution to $\delta\Omega$ of the pseudocontact shift of 25%. Even in this case, the diamagnetic part of $\delta\Omega$ would be equal to ∼2.0 ppm, and this change in chemical shift is large enough to be detected in the reduced form of the protein, if the same conformational exchange process was present. It should be noted, however, that the estimated pseudocontact shift variation is related to a conformational movement of about 1 Å. A larger movement would have larger effects also for the diamagnetic site. As a counter argument, one could also mention that a conformational exchange process was identified for both oxidation states for residue 58 which is characterized by a large variation of the pseudocontact shift within the 40-structure family (0.602 ppm). From the above discussion, we can conclude that the observed difference in mobility between the two oxidation states cannot be simply a result of the pseudocontact shift changes which make "visible" motions in the oxidized state; the same motions would be too small (in terms of $\delta\Omega$) to be detected in the diamagnetic protein.

Comparison of the Detected Motions in the Reduced and Oxidized States of Cyt b_5. The results presented above for the off-resonance rotating frame relaxation behavior of the reduced and oxidized forms of rat microsomal cyt b_5 allow us to compare its dynamic properties in the microsecond to millisecond time scale. The number of backbone nitrogens that display a slow motion is dramatically reduced in the reduced form of the protein with respect to the oxidized one (12 vs 28). A significant comparison can be made for the 25 backbone nitrogens that are commonly assigned. Of those, only 10 experience conformational exchange in both forms, while the remaining 15 display exchange only in the oxidized state. Furthermore, no backbone nitrogen, assigned in both oxidation states, displays slow motions only in the reduced from. Thus, our results provide experimental evidence for increased mobility of the cyt b_5 protein backbone in the oxidized form with respect to the reduced one.

A simple inspection of Table 1 shows that the majority of the backbone nitrogens displaying conformational exchange in the oxidized form are located in helices α3 (six), α4 (four), and α5 (four). Helices α1, α2, and α6 turned out to be less mobile with two, two, and one of their backbone nitrogens, respectively, involved in conformational equilibria. Five other backbone nitrogens characterized by detected motions are located in the four β-strands, while the four remaining backbone nitrogens form part of turns connecting the secondary structural elements. On the other hand, the backbone nitrogens displaying detected motions in reduced cyt b_5 are scattered throughout the protein and are rather evenly distributed between β-strands (four), α-helices (six), and turns (two). The secondary structure element that shows the largest difference in mobility between the two oxidation states is helix α3, which occupies the periphery of one side of the heme-binding pocket and is very rich in acidic residues. In this helix, out of five commonly assigned

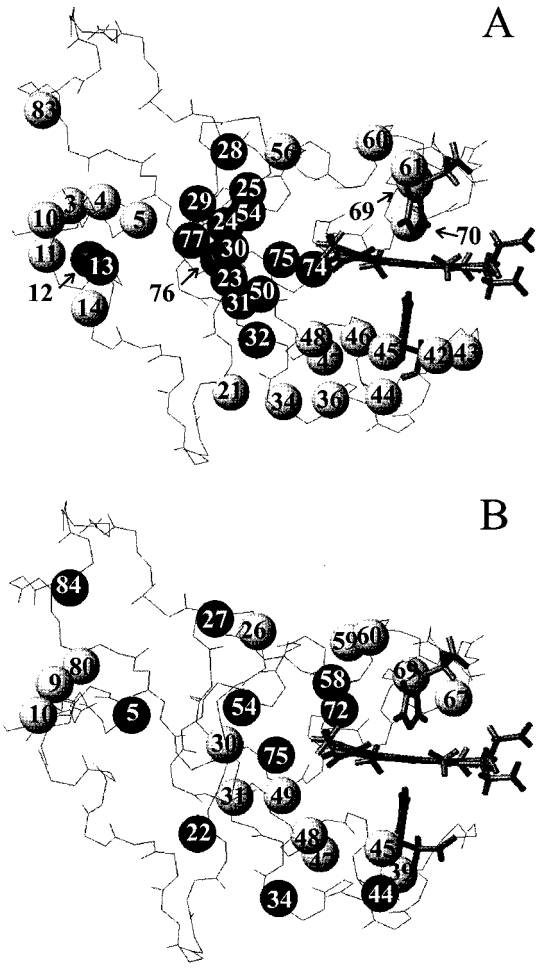

FIGURE 5: Information on the local mobility of rat microsomal cyt b_5 obtained from the exchange behavior of labile protons with the bulk solvent (A) and through $R_{1\rho}$ (B). (A) Black spheres represent residues that were found to be nonexchanging in both oxidation states, while gray spheres represent those that, under the same experimental conditions, were found to be nonexchanging only in the reduced state. (B) Black spheres represent residues for which slow motions were identified in both oxidation states, whereas gray spheres represent those that display a slow motion only in the oxidized state. Therefore, in both cases, gray spheres represent residues that show an oxidation state-dependent local mobility. Black spheres indicate residues that have a common behavior regarding local mobility in both oxidation states. In panel A, they indicate residues that are more "rigid" in both oxidation states while in panel B residues that are more "mobile" in both oxidation states. The average minimized solution structure of oxidized rat microsomal cyt b_5 was used to map the local mobility in the protein frame. Only backbone atoms (including amide protons), the heme, and the two iron binding histidines are shown.

backbone nitrogens, five in the oxidized form and only one in the reduced form display a slow motion.

It is worth comparing the data about local mobility obtained through rotating frame relaxation measurements with those previously reported (*7*), obtained from the exchange behavior of labile protons with the bulk solvent. Both sets of data were acquired in both oxidation states for rat microsomal cyt b_5. It is interesting to note that, in both cases, the oxidized form turns out to be more flexible than the reduced one. No residue showing the reverse behavior is observed. To better analyze what happens at the local level, these data are mapped in the protein frame in Figure 5. The upper part shows data from NH exchange behavior and the lower half those from $R_{1\rho}$ experiments. NH moieties characterized by a redox state-dependent behavior ("mobile" in the oxidized state and "non-mobile" in the reduced state, in the respective time scale) are shown as gray spheres. Black spheres instead represent residues having a common behavior in the two oxidation states. However, this common behavior is of different type in the two sets of experiments. In the NH exchange data (upper part), the black color has been used to indicate the residues that are more "rigid" in both oxidation states. In the $R_{1\rho}$ data (lower half), the black color has been used to indicate that these residues exhibit slow motions (in the microsecond to millisecond time scale) in both oxidation states. The first interesting point is that the β-sheet forming the support for the heme binding pocket turns out to be rigid according to NH exchange data, and no slow motions are observed (with the exception of that of residues 30 and 31). This confirms the role of support carried out by this secondary structural element. Among α-helices, two of them, α3 and α4, show a strong correlation between the two data sets, that is, most of their NH groups show a redox state-dependent behavior. These contain several carboxylate residues that are involved in complex formation with cyt *c*. For the other helices, the correlation between the two data sets is not so strong. Some residues displaying a differential behavior in the two oxidation states in one time scale do not in the other, and the reverse also occurs. However, these two data sets need not be correlated, and in any case, no evidence of higher mobility of the reduced form with respect to the oxidized one is observed.

Biological Consequences. After determination of the three-dimensional solution structure of rat microsomal cyt b_5 in both oxidation states present in living organisms (*7*, *8*), the next step in our effort to understand, at the molecular level, how this protein carries out its function is the study of its local mobility. Indeed, fluctuations of a protein through different conformations around the average solution structure, as determined through NMR, could be a key determinant of many of its properties and of subtle features related to its reactivity. In the case of electron transfer proteins, the structure and dynamics of the protein in both oxidation states through which electron transfer is achieved could give precious insights in understanding which are the factors controlling the thermodynamic stability and the redox potential of the protein, and which are the driving forces governing the interaction with the physiological partners as well as which factors modulate the electron transfer rate. Most electron transfer proteins shuttle electrons through two oxidation states one of which is, in most cases, paramagnetic. The solution structure determination of paramagnetic proteins has now become achievable (*2*, *9*−*11*), and thus, structural comparisons can be made. However, there has been so far only a limited amount of experimental studies, concerning only diamagnetic states, aimed at determining the local mobility of electron transfer proteins (*32*−*34*). Recently, studies of the local dynamics of paramagentic proteins with both standard (*59*) and nonstandard methods (*46*, *68*) were attempted as well. In this study, we have analyzed the local mobility of rat microsomal cyt b_5 in both the reduced (diamagnetic) and oxidized (paramagnetic) states via ^{15}N rotating frame relaxation NMR experiments. Thus, valuable information has been obtained on "slow" local motions in the microsecond to millisecond time scale.

Our results show that the β-sheet at the basis of the heme pocket displays limited mobility in this time scale in both oxidation states. Previous data on the exchange behavior of labile protons with the bulk solvent showed that this part of the protein contains nonexchanging amide protons in either oxidation state and thus inferred a higher rigidity for this secondary structural element relative to the rest of the protein (in a longer time scale). The evidence provided in this study is consistent with the proposed (*7*) role of support of the heme pocket played by this element of secondary structure. On the other hand, the backbone amide nitrogen of a considerable number of residues was found to be involved in a conformational exchange process in the microsecond to millisecond time scale. The majority of residues exhibiting local motions, identified through rotating frame relaxation experiments, in the two oxidation states, belong to the four helices which form the heme binding pocket ($\alpha2-\alpha5$) and to helix $\alpha1$. In particular, all amides belonging to helix $\alpha3$ show, in the oxidized state, slow motions with rates of the order of milliseconds or faster, hinting at a collective motion of this element of secondary structure.

Local motions, on a much faster time scale, were recently analyzed through a "long" (2.5 ns) molecular dynamics simulation on cyt b_5 in water at 298 K and pH 6.9 (*69*). These settings match the experimental conditions of our work. The oxidation state of cyt b_5 in the simulation is not clear, but it resembles better the oxidized rather than the reduced one. The aim of that study was to identify "hot" regions with high local mobility that could be relevant for the interaction of cyt b_5 with its physiological partners. Higher mobility was shown to be localized in three regions, residues 10−20 (region 1), 40−52 (region 2), and 65−75 (region 3), with region 2 being the one deviating more from the crystal structure during the course of the simulation. Our experimental observations of local mobility of cyt b_5 in the oxidized state are in very good agreement with the predicted regions of higher mobility in the molecular dynamics simulation, even if in a different time range. Six residues of region 2 (44−49) and five of region 3 (67, 69, 72, 74, and 75) displayed slow motions in the microsecond time scale. Motions in this time scale, associated with chemical shift variations around 2 ppm, as observed in this case, on the basis of theoretical chemical shift calculations (*70*), are expected to involve rotations of backbone dihedral angles on the order of 30−40° or variations in hydrogen bonding distances and angles. Indeed, the observed local motions identified through rotating frame relaxation experiments in the loop of HiPIP I from *E. halophila* (*46*) probably arise from fluctuations between the two stable conformations identified for this loop in the solid state in which the dihedral angles involved change in conformation by 30−90°. For comparison, motions on a time scale faster than the overall rotational correlation time (in the sub-nanosecond time scale) are expected to involve only variations of dihedral angles smaller than 10−15° (*71*).

Probably the most striking result of the present investigation is the fact that the oxidized form of cyt b_5 is characterized by a higher local mobility than the reduced one in the microsecond to millisecond time scale. This fact has been inferred in the past by several indirect pieces of evidence: oxidized cyt b_5 displays lower thermal stability with respect to the reduced form (*72*, *73*), and the rate of heme interconversion between the two forms (A to B) is faster in the oxidized than in the reduced state (*74*). In addition, a higher mobility of the oxidized form was also noted in the study of the exchange behavior of labile protons with the bulk solvent (*7*). Interestingly, an analogous behavior was also observed for the iso-1-cytochrome *c* from *Saccharomyces cerevisiae* (*6*). Rotating frame relaxation experiments with cyt b_5 now confirm this trend; that is, the oxidized state is also more flexible than the reduced one in the microsecond to millisecond time scale.

Local mobility in electron transfer proteins, in particular if they are oxidation state-dependent, could influence the mechanism of protein−protein recognition with the redox partner. In addition, once the complex is formed, it could modulate the electron transfer rate which depends exponentially on the distance between the two redox centers as well as on the possible pathways. Cyt b_5 has been shown to form complexes with several proteins (*75*−*78*). Among these, the most extensively studied is the cyt b_5−cyt *c* complex (*79*, *80*). On the basis of electrostatic considerations, a first model of the complex was proposed by Salemme (*81*), where the positively charged surface of cyt *c* (Lys 13, Lys 27, Lys 72, and Lys 79) interacts with the negatively charged one of cyt b_5 (Glu 44, Glu 48, Glu 56, Asp 57, and Asp 60).

A molecular dynamics simulation performed on the cyt b_5−cyt *c* complex (*28*) showed that it is far from rigid and that some conformations experienced through the simulation could actually contribute to the electron transfer process and affect the electron transfer rate through the fluctuations of the distance between the two redox centers produced by the protein environment.

Our data show a high number of residues exhibiting motions in the microsecond to millisecond time scale, indicating that cyt b_5 is a quite flexible protein. They also show a redox state-dependent behavior with the oxidized form of the protein being more flexible than the reduced form. An analogous trend was observed through the exchange behavior of labile protons with the bulk solvent (*7*). The correspondence between NH mobility in the microsecond to millisecond time scale and NH exchange leads us to propose that the movements are such that the hydrogen bonds involving the NH protons are instantaneously broken and solvent accessible. The fact that both rat microsomal cyt b_5 (*7*) and cyt *c* from *S. cerevisiae* and horse heart (*5*, *6*, *82*) are more flexible in the oxidized than in the reduced form leads us to speculate about a possible role of mobility in molecular recognition. A flexible molecule is more suitable with respect to a rigid one for complex formation with the redox partner. Indeed, it is reasonable that the lifetime of the mobile form (oxidized state) is larger than about 1 ms which is the upper limit for detection of mobility from $R_{1\rho}$ measurements. If oxidized cyt *c* and reduced cyt b_5 are allowed to react, the flexible oxidized protein becomes reduced and rigid upon electron transfer and vice versa for the other protein. More experimental data on the mobility of the various redox partners are needed before any statement on the generality of the model is made.

ACKNOWLEDGMENT

We thank Massimo Lucci and Enrico Morelli for valuable help in the technical aspects of this work and Dr. H. Desvaux

for kindly providing the program using the Monte Carlo approach to fit the experimental data.

REFERENCES

1. Bertini, I., Eltis, L. D., Felli, I. C., Kastrau, D. H. W., Luchinat, C., and Piccioli, M. (1995) *Chem.−Eur. J. 1*, 598−607.
2. Banci, L., Bertini, I., Eltis, L. D., Felli, I. C., Kastrau, D. H. W., Luchinat, C., Piccioli, M., Pierattelli, R., and Smith, M. (1994) *Eur. J. Biochem. 225*, 715−725.
3. Banci, L., Bertini, I., Dikiy, A., Kastrau, D. H. W., Luchinat, C., and Sompornpisut, P. (1995) *Biochemistry 34*, 206−219.
4. Bertini, I., Dikiy, A., Kastrau, D. H. W., Luchinat, C., and Sompornpisut, P. (1995) *Biochemistry 34*, 9851−9858.
5. Banci, L., Bertini, I., Bren, K. L., Gray, H. B., Sompornpisut, P., and Turano, P. (1997) *Biochemistry 36*, 8992−9001.
6. Baistrocchi, P., Banci, L., Bertini, I., Turano, P., Bren, K. L., and Gray, H. B. (1996) *Biochemistry 35*, 13788−13796.
7. Arnesano, F., Banci, L., Bertini, I., and Felli, I. C. (1998) *Biochemistry 37*, 173−184.
8. Banci, L., Bertini, I., Ferroni, F., and Rosato, A. (1997) *Eur. J. Biochem. 249*, 270−279.
9. Banci, L., and Pierattelli, R. (1995) in *Nuclear magnetic resonance of paramagnetic macromolecules* (La Mar, G. N., Ed.) NATO ASI Series, pp 281−296, Kluwer, Dordrecht, The Netherlands.
10. Bertini, I., and Felli, I. C. (1995) *Quad. Ing. Chim. Ital. 9*, 639−648.
11. Bertini, I., and Rosato, A. (1997) in *Molecular Modeling and Dynamics of Bioinorganic Systems* (Banci, L., and Comba, P., Eds.) pp 1−19, Kluwer, Dordrecht, The Netherlands.
12. Bertini, I., Gray, H. B., Lippard, S. J., and Valentine, J. S. Eds. (1994) in *Bioinorganic Chemistry*, University Science Books, Mill Valley, CA.
13. Tainer, J. A., Getzoff, E. D., Alexander, H., Houghten, R. A., Olson, A. J., Lerner, R. A., and Hendrickson, W. A. (1984) *Nature 312*, 127−134.
14. Mathews, F. S. (1985) *Prog. Biophys. Mol. Biol. 45*, 1−56.
15. Lederer, F. (1994) *Biochimie 76*, 674−692.
16. von Bodman, S. B., Schulder, M. A., Jollie, D. R., and Sligar, S. G. (1986) *Proc. Natl. Acad. Sci. U.S.A. 83*, 9443−9447.
17. Ito, A., and Sato, R. (1968) *J. Biol. Chem. 243*, 4922−4923.
18. Spatz, L., and Strittmatter, P. (1971) *Proc. Natl. Acad. Sci. U.S.A. 68*, 1042−1046.
19. Strittmatter, P., and Ozols, J. (1966) *J. Biol. Chem. 241*, 4787−4792.
20. Gray, H. B., and Ellis, W. R., Jr. (1994) in *Bioinorganic Chemistry* (Bertini, I., Gray, H. B., Lippard, S. J., and Valentine, J. S., Eds.) pp 315−364, University Science Books, Mill Valley, CA.
21. Marcus, R. A., and Sutin, N. (1985) *Biochim. Biophys. Acta 811*, 265−322.
22. Canters, G. W., and van de Kamp, M. (1992) *Curr. Biol. 2*, 859−869.
23. Zhou, J. S., and Kostic, N. M. (1992) *J. Am. Chem. Soc. 114*, 3562−3563.
24. Hake, R., McLendon, G., Corin, A., and Holzschu, D. (1992) *J. Am. Chem. Soc. 114*, 5442−5443.
25. Peerey, L. M., Brothers, H. M. I., Hazzard, J. T., Tollin, G., and Kostic, N. M. (1991) *Biochemistry 30*, 9297−9304.
26. Corin, A., McLendon, G., Zhang, Q., Hake, R., Falvo, J., Lu, K. S., Ciccarelli, R. B., and Holzschu, D. (1991) *Biochemistry 30*, 11585−11595.
27. Walker, M. C., and Tollin, G. (1991) *Biochemistry 30*, 5546−5555.
28. Burch, A. M., Rigby, S. E. J., Funk, W. D., MacGillivray, R. T. A., Mauk, M. R., Mauk, A. G., and Moore, G. R. (1990) *Science 247*, 831−833.
29. Mauk, M. R., Mauk, A. G., Weber, P. C., and Matthew, J. B. (1986) *Biochemistry 25*, 7085−7091.
30. Meyer, T. E., Rivera, M., Walker, F. A., Mauk, M. R., Mauk, A. G., Cusanovich, M. A., and Tollin, G. (1993) *Biochemistry 32*, 622−627.
31. Wendoloski, J. J., Matthew, J. B., Weber, P. C., and Salemme, F. R. (1987) *Science 238*, 794−797.
32. Stone, M. J., Chandrasekhar, K., Holmgren, A., Wright, P. E., and Dyson, H. J. (1993) *Biochemistry 32*, 426−435.
33. Kelley, J. J. I., Caputo, T. M., Eaton, S. F., Laue, T. M., and Bushweller, J. H. (1997) *Biochemistry 36*, 5029−5044.
34. Hrovat, A., Blümel, M., Löhr, F., Mayhew, S. G., and Rüterjans, H. (1997) *J. Biomol. NMR 10*, 53−62.
35. Barbato, G., Ikura, M., Kay, L. E., Pastor, R. W., and Bax, A. (1992) *Biochemistry 31*, 5269−5278.
36. Peng, J. W., Thanabal, V., and Wagner, G. (1991) *J. Magn. Reson. 82*, 82−100.
37. Peng, J. W., and Wagner, G. (1992) *J. Magn. Reson. 98*, 308−332.
38. Habazettl, J., Myers, C., Yuan, F., Verdine, G., and Wagner, G. (1996) *Biochemistry 35*, 9335−9348.
39. Zinn-Justin, S., Berthault, P., Guenneugues, M., and Desvaux, H. (1997) *J. Biomol. NMR 10*, 363−372.
40. Akke, M., and Palmer, A. G., III (1996) *J. Am. Chem. Soc. 118*, 911−912.
41. Abragam, A. (1961) in *The Principles of Nuclear Magnetism*, Oxford University Press, Oxford, U.K.
42. Deverell, C., Morgan, R. E., and Strange, J. H. (1970) *Mol. Phys. 18*, 553−559.
43. Wennerström, H. (1972) *Mol. Phys. 1*, 69−80.
44. Davis, D. G., Perlman, M. E., and London, R. E. (1994) *J. Magn. Reson., Ser. B 104*, 266−275.
45. Akke, M., Liu, J., Cavanagh, J., Erickson, H. P., and Palmer, A. G., III (1998) *Nat. Struct. Biol. 5*, 55−59.
46. Banci, L., Felli, I. C., and Koulougliotis, D. (1998) *J. Biomol. NMR* (in press).
47. Shaka, A. J., Keeler, J., and Freeman, R. (1983) *J. Magn. Reson. 53*, 313−340.
48. Morris, G. A., and Freeman, R. (1979) *J. Am. Chem. Soc. 101*, 760−762.
49. Marion, D., and Wüthrich, K. (1983) *Biochem. Biophys. Res. Commun. 113*, 967−974.
50. Peng, J. W., and Wagner, G. (1994) *Methods Enzymol. 239*, 563−596.
51. Guiles, R. D., Basus, V. J., Sarma, S., Malpure, S., Fox, K. M., Kuntz, I. D., and Waskell, L. (1993) *Biochemistry 32*, 8329−8340.
52. Guiles, R. D., Basus, V. J., Kuntz, I. D., and Waskell, L. (1992) *Biochemistry 31*, 11365−11375.
53. Marquardt, D. W. (1963) *J. Soc. Ind. Appl. Math. 11*, 431−441.
54. Press, W. H., Flannery, B. P., Teukolsky, S. A., and Vetterling, W. T. (1988) in *Numerical Recipes in C−The Art of Scientific Computing*, Cambridge University Press, New York.
55. Palmer, A. G., III, Rance, M., and Wright, P. E. (1991) *J. Am. Chem. Soc. 113*, 4371−4380.
56. Peng, J. W., and Wagner, G. (1992) *Biochemistry 31*, 8571−8586.
57. Desvaux, H., Birlirakis, N., Wary, C., and Berthault, P. (1995) *Mol. Phys. 86*, 1059−1073.
58. James, T. L., Matson, G. B., Kuntz, I. D., and Fisher, R. W. (1977) *J. Magn. Reson. 28*, 417−426.
59. Kelly, G. P., Muskett, F. W., and Whitford, D. (1997) *Eur. J. Biochem. 245*, 349−354.
60. Kay, L. E., Torchia, D. A., and Bax, A. (1989) *Biochemistry 28*, 8972−8979.
61. Bertini, I., and Luchinat, C. (1986) in *NMR of paramagnetic molecules in biological systems*, Benjamin/Cummings, Menlo Park, CA.
62. Bertini, I., and Luchinat, C. (1996) *Coord. Chem. Rev. 150*, 1−300.
63. Banci, L., Bertini, I., and Luchinat, C. (1991) in *Nuclear and electron relaxation. The magnetic nucleus-unpaired electron coupling in solution*, VCH, Weinheim, Germany.
64. Banci, L. (1993) *Biol. Magn. Reson. 12*, 79−111.
65. Phillips, W. D., McDonald, C. C., Stombaugh, N. A., and Orme-Johnson, W. H. (1974) *Proc. Natl. Acad. Sci. U.S.A. 71*, 140−143.

66. McLachan, S. J., La Mar, G. N., and Lee, K.-B. (1988) *Biochim. Biophys. Acta 957*, 430−445.
67. Banci, L., Bertini, I., Gori Savellini, G., Romagnoli, A., Turano, P., Cremonini, M. A., Luchinat, C., and Gray, H. B. (1997) *Proteins: Struct., Funct., Genet. 29*, 68−76.
68. Felli, I. C., Desvaux, H., and Bodenhausen, G. (1998) *J. Biomol. NMR* (in press).
69. Storch, E. M., and Daggett, V. (1995) *Biochemistry 34*, 9682−9693.
70. de Dios, A. C., Pearson, J. G., and Oldfield, E. (1993) *Science 260*, 1491−1496.
71. Bruschweiler, R., and Wright, P. E. (1994) *J. Am. Chem. Soc. 116*, 8426−8427.
72. Kitagawa, T., Sugiyama, T., and Yamano, T. (1982) *Biochemistry 21*, 1680−1686.
73. Newbold, R. J., Hewson, R., and Whitford, D. (1992) *FEBS Lett. 314*, 419−424.
74. McLachlan, S. J., La Mar, G. N., Burns, P. D., Smith, K. D., and Langry, K. C. (1986) *Biochim. Biophys. Acta 874*, 274−284.
75. Strittmatter, P., Hackett, C. S., Korza, G., and Ozols, J. (1990) *J. Biol. Chem. 265*, 21709−21713.
76. Poulos, T. L., and Mauk, A. G. (1983) *J. Biol. Chem. 258*, 7369−7373.
77. Mauk, M. R., and Mauk, A. G. (1982) *Biochemistry 21*, 4730−4734.
78. Stayton, P. S., Poulos, T. L., and Sligar, S. G. (1989) *Biochemistry 28*, 8201−8205.
79. Rodgers, K. K., Pochapsky, T. C., and Sligar, S. G. (1988) *Science 240*, 1657−1659.
80. Northrup, S. H., Thomasson, K. A., Miller, C. M., Barker, P. D., Eltis, L. D., Guillemette, J. G., Inglis, S. C., and Mauk, A. G. (1993) *Biochemistry 32*, 6613−6623.
81. Salemme, F. R. (1976) *J. Mol. Biol. 102*, 563−568.
82. Marmorino, J. L., Auld, D. S., Betz, D. S., Doyle, D. F., Young, G. B., and Pielak, G. J. (1993) *Protein Sci. 2*, 1966−1974.

BI980885F